Controlling Shell Thickness in Core−Shell Gold Nanoparticles via Surface-Templated Adsorption of Block Copolymer Surfactants

Youngjong Kang and T. Andrew Taton*

Department of Chemistry, University of Minnesota, 207 Pleasant St SE, Minneapolis, Minnesota 55455

Received February 24, 2005; Revised Manuscript Received April 19, 2005

ABSTRACT: When Au nanoparticles are encapsulated within shells of cross-linked, block copolymer amphiphiles, the structure of the shells is determined by the initial interaction between the amphiphile and the nanoparticle surface. In the case of small nanoparticles, for which particle size is comparable to the dimension of the block copolymer ($\rho_{Au}/R_g \approx 1$), particles act like solutes that are dissolved within polystyrene-*block*-poly(acrylic acid) (PS-*b*-PAA) micelle cores. In the case of larger nanoparticles ($\rho_{Au}/R_g > 1$), PS-*b*-PAA adsorption is templated by the particle surface, and a concentric core−shell structure is formed. The thickness of this shell can be predicted from theoretical models of polymer adsorption onto highly curved surfaces and controlled by varying the ratio of polymer to available nanoparticle surface area. We anticipate that these rules will illustrate how cross-linked copolymer shells with predetermined thickness can be used to stabilize and functionalize a variety of nanoparticle materials.

Introduction

Amphiphilic block copolymers have been studied extensively for their ability to self-assemble in selective solvents and form stable micelles and adsorbed monolayers at very low polymer concentrations. This property makes amphiphilic block copolymers very effective surfactants and enables them to solubilize and stabilize otherwise insoluble substances in various media as vehicles for drug delivery,[1−4] as microreactors for chemical synthesis and catalysis,[5] and as general detergents.[6] Block copolymers also have been used to compatibilize surfaces and colloidal particle suspensions by surface adsorption in selective solvents.[7,8] The theories that describe the selective adsorption of block copolymers at surfaces and the selective solvation of solutes into block copolymer micelles have important differences. For the case of incorporation of molecular solutes within surfactant micelles, theory predicts that added solute will progressively perturb the original structure of the polymer micelle by swelling the interior.[9−11] Nevertheless, if the concentration of solute is low, the structure of the surfactant micelle is still largely dictated by the molecular properties of the copolymer alone. By contrast, the assembly of polymer surfactants at macroscopic surfaces in selective solvents is dependent on a number of factors, including the relative affinity of each polymer block for the surface and for solvent, block lengths and fractions, interfacial surface area, and polymer concentration.[12−17] These effects can have a considerable effect on the thickness and regularity of the assembled surfactant layer. An important assumption of most theories on adsorption is that curvature of the surface is small relative to polymer chain length and film thickness. As a result, it is not clear what sort of monolayer structure should be formed by block copolymer assembly on the highly curved surface of a nanoparticle—an adsorbate layer, a micelle, or something in between. Bates, Tirrell, and co-workers have estimated that surface curvature affects adlayer thickness when the radius of curvature approaches the radius of gyration of the polymer ($\rho/R_g \approx 1$).[15] Theoretical work by Qiu and Wang likewise suggests that there is a range of particle sizes over which polymer surfactants exhibit a combination of surface adsorption and micellization.[16] Intuitively, the assembly of block copolymer surfactants onto a nanoparticle surface should look more like a grafted layer when the particle is large and more like a micelle when the particle is small. Very little experimental work has been done to characterize this particle size regime.[17]

Block copolymer surfactants have played a particularly important role in the development of nanoparticles as technological tools. The inherently large surface area-to-volume ratio of nanoparticles gives them high surface energies and low stability in suspension without stabilizers. Block copolymers have been used to stabilize a variety of nanoparticle materials by forming steric or ionic barriers around the particles.[18−23] In general, nanoparticles are better stabilized by thicker and denser polymer shells, which result in strong depletion stabilization.[12,13] As part of an effort to functionalize and stabilize inorganic nanoparticles, we have previously reported that nanostructures captured within block copolymer shells can be further stabilized by chemically cross-linking the surrounding surfactant into a permanent structure.[24] For example, a shell of amphiphilic poly(styrene-*block*-acrylic acid) (PS-*b*-PAA) surrounding Au nanoparticles in water could be permanently fixed by cross-linking the outer PAA blocks.[25] Originally, a micelle solvation model was invoked to predict the polymer layer thickness and amount of polymer required for encapsulation. However, the validity of this model was observed to depend very sensitively on the size of the nanoparticles. Larger nanoparticles acted more like flat surfaces than molecular solutes with respect to the surface assembly of polymer molecules, and the thickness of the adsorbed polymer layer was observed to vary significantly with polymer concentration and solvent conditions. Modulating the thickness of the cross-linked copolymer layer would provide further control over the chemical and physical properties of surfactant-encapsulated nanostructures.

The adsorption of block copolymers on flat surfaces and large colloidal particles in selective solvents has

* Corresponding author: e-mail taton@chem.umn.edu.

10.1021/ma050400c CCC: $30.25
Published on Web 06/16/2005

Scheme 1

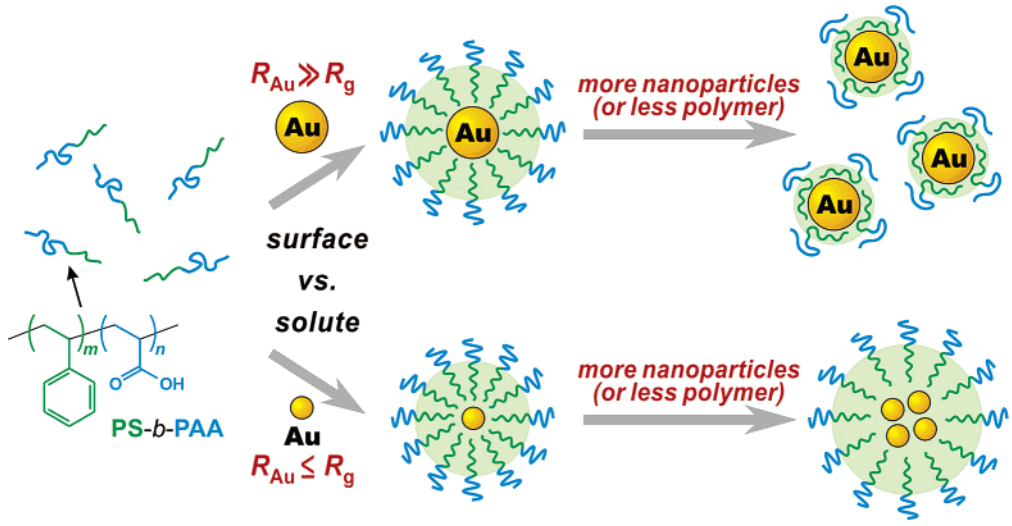

been theoretically described by Marques, Joanny, and Leibler[14] in terms of the relative energies of interactions between the copolymer, surface, and solvent. The adsorbed copolymer layer is in equilibrium with free polymer in the solution reservoir (often in the form of micelles), and the amount of adsorbed polymer and the layer thickness is determined by a thermodynamic energy balance between the chemical potential of the reservoir solution, the free energy of the desolvated grafted polymer block, and the stretching energy of the solvated polymer block. Marques described a number of different regimes of interaction where different energies predominate. The copolymer layer thickness (t_{shell}) is small at low polymer concentration or when the adsorbed block is weakly desolvated. Conversely, t_{shell} is maximized at high polymer concentrations or when the adsorbed copolymer is strongly desolvated. However, these studies have focused on the self-assembly of copolymers on macroscopic surfaces.

In this study we show that the Marques−Joanny−Leibler (MJL) model of surfactant adsorption accurately describes the thickness of cross-linked, block copolymer nanoshells. For PS-*b*-PAA copolymers, the grafting model generally describes the behavior of polymer adsorption to nanoparticles as small as 10 nm in diameter (Scheme 1). Because the thickness of the adsorbed polymer layer does not change during cross-linking, the eventual structure of the cross-linked shell is determined not only by the macromolecular characteristics of the copolymer but also by the initial adsorption conditions. As predicted by MJL theory, t_{shell} is greatest at a low ratio of nanoparticles to copolymer and smallest at high ratios. This concept has been used to coat Au nanoparticles with shells of predictable thickness ranging from 10 to 40 nm. Particles smaller than 10 nm, however, act more like solutes than surfaces, and reduction of the polymer concentration increased the number of particles within micelles rather than decreasing polymer layer thickness. We argue that this observation confirms theoretical prediction that too much surface curvature can lead to incomplete coverage by adsorbed surfactants.

Experimental Section

Synthesis and Characterization. Polystyrene-*block*-poly(acrylic acid) (PS-*b*-PAA) was synthesized via sequential atomic transfer radical polymerization (ATRP) of *tert*-butyl acrylate and styrene to PS-*b*-P*t*BA, followed by deprotection of *tert*-butyl groups to yield PS-*b*-PAA.[25−27] Molecular weight characterization data of polymers are summarized in Table 1. Au nanoparticles (12.3 ± 1.1, 31.0 ± 2.5, or 51.4 ± 4.8 nm, determined by TEM) were prepared by trisodium citrate reduction[28] or by seeded growth.[25,29]

Table 1. Molecular Weight Characterization Data of PS-*b*-PAA Amphiphiles[a]

polymer composition	$M_n \times 10^{-3}$ (g/mol)	$M_w \times 10^{-3}$ (g/mol)	PDI
PS_{100}-*b*-PAA_{13}	11.8	13.5	1.14
PS_{160}-*b*-PAA_{13}	17.6	19.6	1.11
PS_{250}-*b*-PAA_{13}	26.8	30.8	1.15

[a] Values derived from GPC analysis of precursor PS-*b*-P*t*BA polymers.

Transmission electron microscopy (TEM) images were obtained on a JEOL 1210 electron microscope equipped with a Gatan video camera and a Gatan Multiscan CCD camera (1024 × 1024 pixels). TEM samples were prepared by dropping nanoparticle solutions (5 μL) onto Formvar-graphite-coated copper grids (300 mesh, Electron Microscopy Science) and air-drying. All TEM images were obtained at an operating voltage of 120 kV.

Encapsulation of Au Nanoparticles. Au nanoparticles dispersed in DMF were prepared by centrifugation and redispersion of citrate-stabilized, aqueous Au nanoparticles.[25] Encapsulation of these particles within PS-*b*-PAA was performed according to a previously reported method[25] with modified reagent ratios and reaction times. To encapsulate Au nanoparticles within PS_{100}-*b*-PAA_{13}, 10 μL of PS_{100}-*b*-PAA_{13} solution (10^{-2} g/mL in DMF) was added to 1.0 mL of Au nanoparticle solution (d_{Au} = 31 nm, 648 pM in DMF) with vigorous stirring. In this step, the concentration of Au nanoparticle solution could be varied, with the polymer concentration held constant to change the ratio of polymer to particles. Then, 200 μL of H_2O was gradually added dropwise (8.3 μL/min) via syringe pump with continued stirring. At this point, the solution turned slightly violet in color and became deeper violet as more H_2O was added. After 10 min, 5 μL of dodecanethiol solution (1 vol % in DMF) was also added to the solution, and then the resulting solution was stirred for 24 h. Nanoparticles were diluted with H_2O, purified by dialysis, cross-linked, and separated from empty micelles by centrifugation as previously described.[25] For cross-linking, 0.5 equiv of 1-(3-dimethylamino)propyl)-3-ethylcarbodiimide methiodide activator and 1.0 equiv of 2,2′-(ethylenedioxy)bis(ethylamine) difunctional linker were used, calculated on the basis of the number of reactive PAA groups. Encapsulation with PS_{160}-*b*-PAA_{13} and PS_{250}-*b*-PAA_{13}, or with different size Au nanoparticles, was performed similarly.

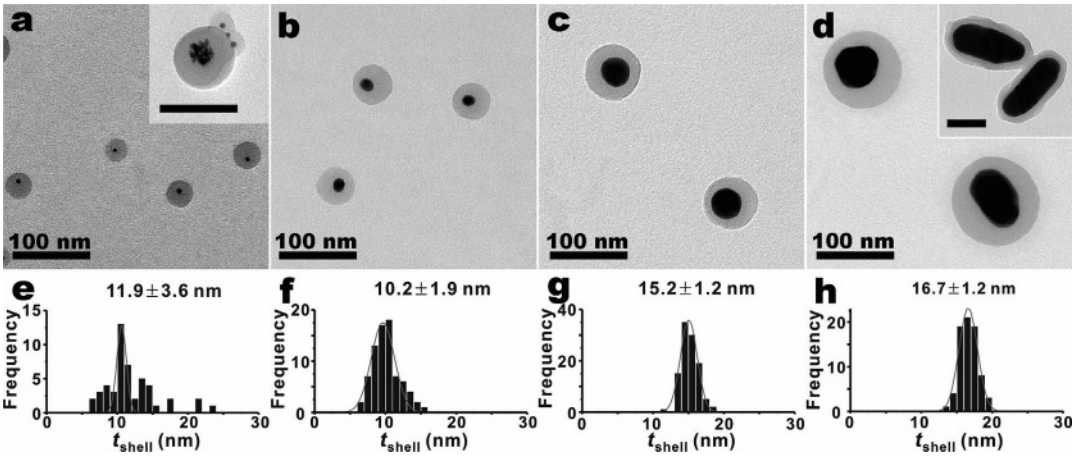

Figure 1. TEM images (a−d) and histograms of shell thickness (e−h) for Au@PS_{100}-*b*-PAA_{13} with different core diameters: d_{Au} = (a, e) 4.1 ± 0.5 nm, (b, f) 12.3 ± 1.1 nm, (c, g) 31.0 ± 2.5 nm, and (d, h) 51.4 ± 4.8 nm. (Inset, a) Typical TEM image of micelles filled with multiple 4 nm Au nanoparticles, observed in the same sample as (a). Scale bar represents 100 nm. (Inset, d) Typical TEM image of the encapsulated Au nanorods (d = 100 nm, l = 300 nm). Scale bar represents 100 nm. For all samples, the initial polymer concentration was $[PS_{100}\text{-}b\text{-}PAA_{13}]_{initial} = 10^{-4}$ g/mL = $6.7 n_m^s A_{Au}^{total}$. See Supporting Information for other TEM images used to obtain histograms.

Results and Discussion

Correlation of Cross-Linked Shell Thickness and Surfactant Adsorption. The overall goal of this study was to determine what factors could be used to control the thickness of cross-linked surfactant shells surrounding nanoparticles. These core−shell nanostructures were fabricated by (1) dissolving the nanoparticle and surfactant in DMF, a solvent that is good for both solutes, (2) gradually adding water to induce surfactant assembly around the nanoparticle, and (3) fixing the surfactant layer by chemical cross-linking. In this study, we have used TEM of structures after cross-linking as an indicator of how surfactant interacts with nanoparticles before cross-linking. On the basis of previous studies of empty cross-linked copolymer micelles by Wooley[30] and Liu,[31] we assume that the structure of the shell does not change during the cross-linking process. This assumption should be correct only if fluctuation of the assembled surfactant structure occurs much more slowly than cross-linking. For micelles and surfactant layers made from PS-*b*-PAA, the hydrophobic PS core is glassy and rigid under the aqueous conditions used to cross-link the PAA shell.[32] For samples in which excess PS-*b*-PAA surfactant was added to Au nanoparticles to form thick protective shell, TEM images obtained before cross-linking the assembled shells were essentially identical to those obtained after cross-linking.[33] However, for samples in which the ratio of polymer to nanoparticles was not large (which comprise many of those described in this study), the un-cross-linked surfactant shells fused and aggregated during isolation and TEM sample preparation. As a result, we have made the assumption that the structures observed by TEM after cross-linking reflect the way surfactant adsorbs before cross-linking. We have also assumed that, although the glassy PS core freezes the surfactant shell in place, that the observed structures represent thermodynamic rather than kinetically trapped states of the shell. Eisenberg and co-workers have previously characterized the conditions under which PS-*b*-PAA surfactants assemble into kinetic or thermodynamic structures.[34] To ensure thermodynamic equilibrium between copolymer adsorbed onto the Au particle surface and the reservoir of copolymer in solution, the mixture was first allowed to stir for 24 h at low water fraction (wc = 15−20%), where micelles form but the PS core is still slightly solvated, before completing the transfer to water. In this way, we expected to avoid the complex kinetic structures that Eisenberg has observed for PS-*b*-PAA micelles when solvent polarity is changed more rapidly.[35]

Dependence of Encapsulation on Nanoparticle Size. To determine the effect of surface curvature on the structure of cross-linked core−shell nanoparticles, we first characterized Au nanoparticles encapsulated with PS_{100}-*b*-PAA_{13} ("Au@PS_{100}-*b*-PAA_{13}") for several different sizes of nanoparticle (ρ_{Au} = 2−60 nm). In this system, the nanoparticle radii are comparable to the dimensions of the polymer chains ($R_g \approx 3$ nm for PS_{100}-*b*-PAA_{13}), and so the particles could act as solutes or surfaces with respect to the surfactant during surfactant adsorption. We defined monolayer capacity n_m^s for each nanoparticle size as the amount of copolymer required to form a monolayer on a 1 nm^2 area of particle with a thickness equivalent to the theoretical root-mean-square end-to-end distance ($\langle h^2 \rangle_0^{1/2}$) of an unperturbed polymer chain. The value of n_m^s increases slightly with increasing surface curvature. To make a consistent comparison, the ratio of polymer concentration to monolayer capacity and total surface area of added Au particles ($A_{Au}^{total} = A_{Au} N_a$[Au], where A_{Au} is surface area of an Au nanoparticle, N_a is Avogadro's number, and [Au] is the concentration of Au nanoparticles) was set to be the same ($[PS_{100}\text{-}b\text{-}PAA_{13}]_{initial} = 10^{-4}$ g/mL = $6.7 n_m^s A_{Au}^{total}$), and in considerable excess, for experiments on particle size dependence. In other words, the amount of added polymer was 6.7 times that required to form a complete monolayer around each Au nanoparticle. Under these conditions, the excess surfactant reservoir consists primarily of empty micelles due to the remarkably low critical micelle concentration of the copolymer.

For Au nanoparticles 12 nm in diameter or larger ($\rho_{Au}/R_g \geq 1$, Figure 1b−d), each core−shell structure consisted of exactly one nanoparticle surrounded by a shell of fairly consistent thickness. We considered that a statistical distribution of particles encapsulated within micelles might lead to a few structures containing two or more particles. No such structures, however, were observed. Even extremely large and irregularly shaped

nanoparticles were passivated with shells that appeared very similar to those surrounding 12 nm particles (Figure 1d). For smaller nanoparticles (4 nm diameter, $\rho_{Au}/R_g \approx 1$), on the other hand, some structures did indeed contain multiple particles (Figure 1a), under the same encapsulation conditions as the bigger particles. Similar characteristics of multiple nanoparticles solvated within polymer surfactant micelles have been reported.[36,37] In addition, the variation of average surface thickness among particles was much larger for smaller nanoparticles than for larger ones and approached the variation observed in free PS_{100}-*b*-PAA_{13} micelles.

These differences indicate that 4 and 31 nm diameter nanoparticles span the range over which PS_{100}-*b*-PAA_{13} either solvates the particle as solute or adsorbs to the particle as a surface. Small Au nanoparticles behaved like solutes, swelling the micelle core. These particles were statistically partitioned into the cavities of the micelle cores, and micelles containing more nanoparticles were reproducibly larger than those with fewer particles. As a result, this random distribution of particles led to micelles having very broad size distribution (Figure 1e), as is commonly observed for solute-swollen micelles.[38,39] These observations demonstrated that it would be difficult to generate monodisperse samples of singly encapsulated, small Au particles using PS_{100}-*b*-PAA_{13}. Changing the encapsulation conditions—including relative and absolute polymer and particle concentrations, solvent composition, and transitions—failed to improve the quality of encapsulated, small particles. If the mechanism of surfactant adsorption was indeed related to ρ_{Au}/R_g, then reducing the molecular weight of the polymer should have improved encapsulation; however, particles smaller than 10 nm in diameter were insufficiently stabilized by shorter PS-*b*-PAA surfactants.

By contrast, encapsulated nanostructures observed with nanoparticles larger than 10 nm in diameter were reproducibly and singly encapsulated within cross-linked PS_{100}-*b*-PAA_{13}, and the thickness of the shell was consistent with surfactant adsorption onto a curved nanoparticle surface. For larger particles, shell thickness gradually increased with increasing nanoparticle diameter when the ratio of polymer to particle surface area was kept constant (Figure 1f–h). Although the range of shell thickness was small, it was larger than measurement error and variation from sample to sample (<1 nm). The same trend has been characterized for copolymer adsorption onto curved surfaces[17,40–43] and has been explained in terms of a simple blob model of adsorbed polymer chain conformation.[13,44] According to this model, decreasing the surface curvature should increase segment–segment interaction in the polymer layer, decrease blob size, and increase the resulting layer thickness. Our experimental results agree with this theoretical expectation. Another way to express variation of adlayer thickness is in terms of stretching of the adsorbed polymer chains,[45] which is induced by increasing segment–segment interactions between polymer molecules. Here, we have defined the degree of stretching of the PS block (S_{PS}) as the ratio of measured shell thickness (t_{shell}) to $\langle h^2\rangle_0^{1/2}$. As summarized in Table 2, the degree of stretching of PS blocks (S_{PS}) increased with increasing nanoparticle diameter, but the surface density of chains (σ) remained constant. For chains adsorbed to 12 nm Au nanoparticles, the value of S_{PS} is as small as that of empty PS-*b*-PAA micelles,[34] but chains encapsulating larger Au nanoparticles exhibited significantly higher S_{PS} values. The surface densities σ for chains encapsulating all Au nanoparticles larger than 10 nm are, on the other hand, almost identical. In our previous report,[25] images of encapsulated 12 and 31 nm Au nanoparticles showed the same shell thickness; in these past experiments, we failed to control the ratio of polymer to surface area, and we argue that the similarity in shell thickness for these preparations was coincidental. By contrast, we report here that keeping $[\text{PS-}b\text{-PAA}]/n_m^s A_{Au}^{total}$ constant results in identical surface density, and thus different shell thickness, for different Au nanoparticle sizes. The calculated degree of stretching and surface density for encapsulated 4 nm Au (Table 2) deviate substantially from this trend, consistent with the hypothesis that these smaller particles are dissolved in micelles rather than passivated by an adlayer. Taken together, the experimental results on varying nanoparticle size demonstrate that, for particles encapsulated within a complete cross-linked surfactant monolayer, shell thickness is determined by stretching of polymer chains induced by surface curvature rather than by variation in surface coverage. In addition, these results suggest guidelines for protecting a wide range of nanoparticle sizes with cross-linked amphiphile shells.

Table 2. Characteristics of Au@PS_{100}-*b*-PAA_{13} with Different Nanoparticle Core Sizes

d_{Au} (nm)	t_{shell} (nm)	S_{PS}[a]	σ[b]
4.1 ± 0.5	11.9 ± 3.6	1.77	0.84
12.3 ± 1.1	10.2 ± 1.9	1.52	0.13
31.0 ± 2.5	15.2 ± 1.2	2.25	0.13
51.4 ± 4.8	16.7 ± 1.2	2.49	0.12

[a] Degree of stretching of PS blocks, taken as the ratio of t_{shell} to the end-to-end distance of the PS block $\langle h^2\rangle_0^{1/2} = b\sqrt{N_{PS}}$, where b is the statistical segment length (6.7 Å for PS) and N_{PS} is degree of polymerization of PS.[46,47] [b] Surface density, defined as $\sigma = (N_{agg} \times a^2)/A_{Au}$, where N_{agg} is the aggregation number of polymer chains absorbed on the surface of an Au nanoparticle, a is the monomer length (2.5 Å for styrene), and A_{Au} is the surface area of one Au nanoparticle.[14] Italicized values vary significantly from the observed trend.

Influence of Surface Area on Shell Thickness. When particle encapsulation is best described by an adsorption model (for $\rho_{Au}/R_g \gg 1$), the structure of the polymer adlayer is significantly affected by the available surface area. To investigate this effect, Au nanoparticles ($\rho_{Au} = 15.5$ nm) were encapsulated with PS_{100}-*b*-PAA_{13} at various ratios of polymer to total particle surface area. This ratio was varied by adding different amount of nanoparticles while keeping the initial polymer concentration constant ($[PS_{100}\text{-}b\text{-}PAA_{13}]_{initial} = 10^{-4}$ g/mL). Experiments were performed such that $[\text{PS-}b\text{-PAA}]/n_m^s A_{Au}^{total}$ ranged from 2.60 to 325.

As shown in Figure 2, the shell thickness of the encapsulated nanoparticle gradually increased with increasing $[\text{PS-}b\text{-PAA}]/n_m^s A_{Au}^{total}$ ratio. Averaged over 100 particles, the shell thicknesses for Au@PS_{100}-*b*-PAA_{13} ($d_{Au} = 31$ nm) increased from 8.9 ± 1.0 to 40.1 ± 2.0 nm as $[\text{PS-}b\text{-PAA}]/n_m^s A_{Au}^{total}$ increased from 2.6 to 325. This overall increase in shell thickness was accompanied by an increase in the number of empty micelles remaining in the encapsulation solution, as observed in TEM images of unpurified material.[33] Both of these observations can be understood in terms of the MJL model of surfactant adsorption.[14] According to this

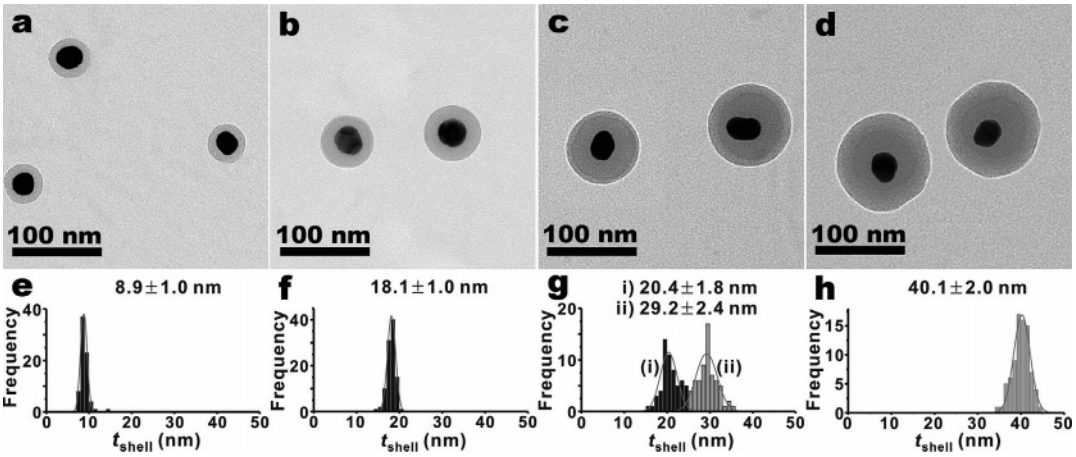

Figure 2. TEM images (a−d) and histograms of shell thickness (e−h) for Au@PS_{100}-*b*-PAA_{13}, $d_{Au} = 31$ nm, with varying polymer to surface area. $[PS_{100}\text{-}b\text{-}PAA_{13}]/n_m^s A_{Au}^{total}$ = (a, e) 2.6, (b, f) 13, (c, g) 65, and (d, h) 325. Histogram (g) represents two populations of single-layered (black) and double-layered (grey) structures. Image (d) and histogram (h) shows double-layered structures only. The initial polymer concentration was $[PS_{100}\text{-}b\text{-}PAA_{13}]_{initial} = 10^{-4}$ g/mL for all samples. See Supporting Information for other TEM images which were used in obtaining histograms.

Table 3. Dependence of the Structure of Adsorbed Polymer Layer on $[PS\text{-}b\text{-}PAA]/n_m^s A_{Au}^{total}$ Ratio

$[PS_{100}\text{-}b\text{-}PAA_{13}]/n_m^s A_{Au}^{total}$	t_{shell} (nm)	S_{PS}[a]	σ[b]
325	40.1 ± 2.0[c]	*5.98*[c]	*0.87*[c]
65	29.2 ± 2.4[c]	*4.36*[c]	*0.44*[c]
	20.4 ± 1.8	3.04	0.22
13	18.1 ± 1.0	2.70	0.18
6.5	14.9 ± 1.1	2.22	0.13
4.3	13.5 ± 1.6	2.01	0.11
3.2	12.4 ± 2.0	1.85	0.09
2.6	8.9 ± 1.0	1.32	0.06

[a,b] See Table 2 for definitions. [c] Values are for nanoparticles encapsulated within double-layered polymer shells. Italicized values vary significantly from the observed trend.

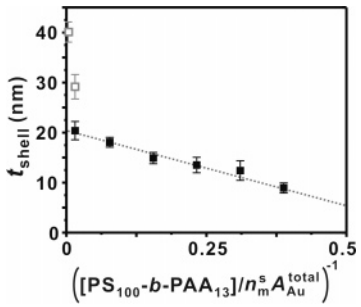

Figure 3. Variation of shell thickness with $([PS_{100}\text{-}b\text{-}PAA_{13}]/n_m^s A_{Au}^{total})^{-1}$: (■) t_{shell} measured for particles showing a single shell layer; (□) t_{shell} measured for particles showing a double-layered shell. A linear fit to the data for single-layered shells gave slope −14.4 nm and $R = -0.99$.

equilibrium model, the adlayer thickness is related to the effective chemical potential exerted on the available surface area by the reservoir of available polymer. As a result, during nanoparticle encapsulation, the shell thickness should be dependent not on the absolute concentration of polymer or Au nanoparticle but on the relative amount of polymer and Au nanoparticle. We observed that varying [PS-*b*-PAA] over an order of magnitude yielded Au@PS-*b*-PAA with the same shell thickness as long as $[PS\text{-}b\text{-}PAA]/n_m^s A_{Au}^{total}$ was kept constant. Varying the $[PS\text{-}b\text{-}PAA]/n_m^s A_{Au}^{total}$ ratio, however, yielded consistent changes in surface density of adsorbed polymer and in chain stretching. As $[PS\text{-}b\text{-}PAA]/n_m^s A_{Au}^{total}$ was increased, both σ and S_{PS} increased continuously (Table 3). Interestingly, we also found that shell thickness exhibited a linear relationship with $([PS\text{-}b\text{-}PAA]/n_m^s A_{Au}^{total})^{-1}$ for a broad range of $[PS\text{-}b\text{-}PAA]/n_m^s A_{Au}^{total}$ ratios (Figure 3). We have found that this linear relationship allows us to predictably control the shell thickness of the produced Au@PS-*b*-PAA by simply varying the relative concentration of polymer and available particle surface area.

At high $[PS\text{-}b\text{-}PAA]/n_m^s A_{Au}^{total}$ ratios, the relationship between shell thickness and $([PS\text{-}b\text{-}PAA]/n_m^s A_{Au}^{total})^{-1}$ deviated from this trend, and TEM images showed some particles with double layers of slightly different contrast. Samples of Au@PS_{100}-*b*-PAA_{13} prepared at $[PS\text{-}b\text{-}PAA]/n_m^s A_{Au}^{total} = 65$ contained a mixture of single- and double-layered particles (Figure 2c,g), and particles prepared with much higher $[PS\text{-}b\text{-}PAA]/n_m^s A_{Au}^{total}$ ratios were entirely double-layered (Figure 2d,h). In all of these cases, the total multilayer shell thickness was larger than the theoretical length of a fully stretched PS_{100}-*b*-PAA_{13} chain (26 nm). Although we have previously observed layered structures in TEM images of copolymer micelles that are swollen with small-molecule solute, empty micelles from unpurified material from these preparations looked normal.

The organization of the polymer in these layered structures is not clear. In particular, we do not understand how an additional layer of block amphiphile could assemble onto a hydrophilic surface to yield another hydrophilic surface. So, the composition of these double-layered structures and the mechanism of their formation are still under investigation in our lab. Nonetheless, the size polydispersity of these shells is still exceptionally low, and encapsulating particles within amphiphile multilayers extends our ability to control to control polymer thickness in Au-core/copolymer-shell nanostructures.

Effect of Polymer Composition on Shell Thickness. The relative and absolute lengths of the copolymer blocks also greatly affected the structure of the adsorbed polymer layer. We previously reported that we could only successfully encapsulate Au nanoparticles with highly asymmetric block copolymers.[25] TEM images of nanoparticles mixed with moderately asymmetric or symmetric copolymers (PS_{159}-*b*-PAA_{62}, PS_{49}-*b*-PAA_{54}) failed to show adsorption of polymer to particle surfaces,

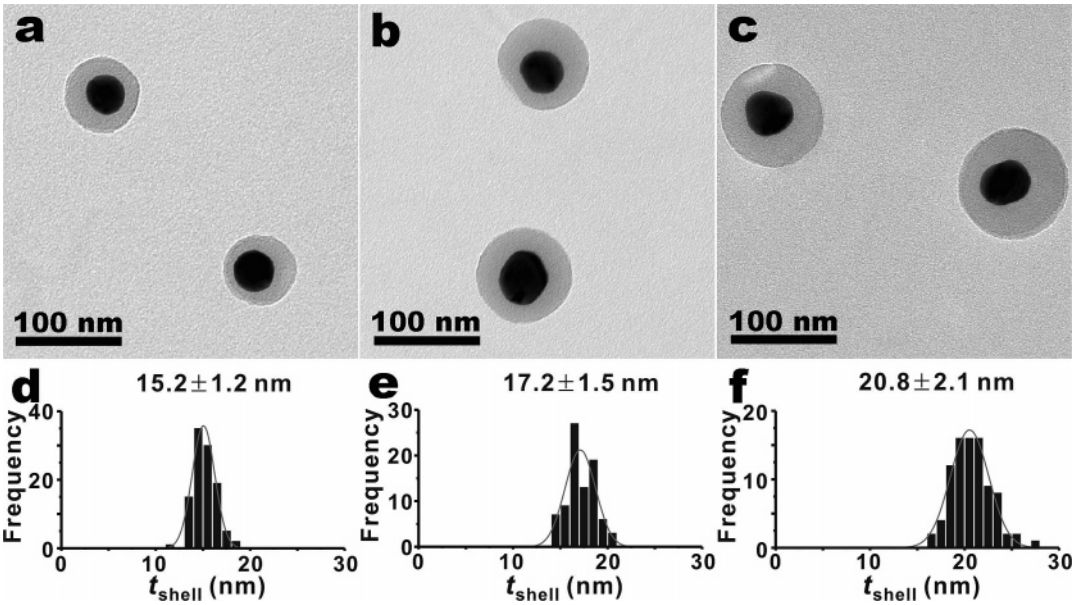

Figure 4. TEM images (a−c) and histograms of shell thickness (d−f) of encapsulated 31 nm Au nanoparticles within micelles formed with (a) PS_{100}-*b*-PAA_{13}, (b) PS_{160}-*b*-PAA_{13}, and (c) PS_{250}-*b*-PAA_{13}. The initial polymer concentration was $[PS\text{-}b\text{-}PAA]_{initial} = 10^{-4}$ g/mL $= 6.7 n_m^s A_{Au}^{total}$ for all samples. All empty micelles were completely removed by 3−5 times of consecutive centrifugations after cross-linking the acrylate groups in PAA blocks by 50%. See Supporting Information for other TEM images which were used in obtaining histograms.

Table 4. Dependence of the Shell Thickness on Polymer Composition

polymer composition	t_{shell} (nm)	S_{PS}[a]	σ[b]
PS_{100}-*b*-PAA_{13}	15.2 ± 1.2	2.27 (1.52[c])	0.13
PS_{160}-*b*-PAA_{13}	17.2 ± 1.5	2.03	0.10
PS_{250}-*b*-PAA_{13}	20.8 ± 2.1	1.96 (1.43[c])	0.09

[a,b] See Table 2 for definitions. [c] Values are for empty micelles isolated from the encapsulated nanoparticle solution.

whereas very asymmetric polymers (PS_{250}-*b*-PAA_{13}, PS_{160}-*b*-PAA_{13}, PS_{100}-*b*-PAA_{13}, $PMMA_{240}$-*b*-PAA_{13}) successfully formed thick surfactant shells. This difference could be explained by competition between adsorption of copolymer onto the nanoparticle surface and formation of empty micelles in solution by surfactant molecules.[16,48,49] Qualitatively, when other factors are same, polymers having longer hydrophobic blocks are predicted to favor adsorption, and polymers having longer hydrophilic blocks should favor self-association into micelles in aqueous solution.[16] Within the range of surfactants that successfully formed shells around nanoparticles, we found that shell thickness could be further controlled by copolymer composition. At constant $[PS\text{-}b\text{-}PAA]/n_m^s A_{Au}^{total}$ (=6.7), the shell thickness of Au@PS-*b*-PAA (d_{Au} = 31 nm) increased from 15.2 ± 1.2 to 20.8 ± 2.1 nm as the PS block length increased from N_{PS} = 100 to N_{PS} = 250 (Figure 4). A number of relationships between surface-grafted polymer layer thickness and polymer molecular weight have been proposed; Marques et al. predicted $t_{shell} \propto N^{1/2}$ at flat surfaces,[14] and Ligoure and Liebler subsequently predicted $t_{shell} \propto N^{3/5}$ at curved surfaces,[50] for polymers with identical surface density. The three samples we evaluated for PS_N-*b*-PAA_{13} more closely fit the relationship $t_{shell} \propto N^X$ with $X \approx 1/3$, but the calculated surface density for this series also varies (Table 4). More importantly, the shell thickness for Au@PS_N-*b*-PAA_{13} progressively increases with increasing surfactant molecular weight N, as predicted by adsorption theory.

Conclusions

The present study shows that for Au nanoparticles larger than 10 nm in diameter a general polymer adsorption model successfully describes the formation of well-defined core−shell Au nanoparticles (Au@PS-*b*-PAA). The structures of these core−shell nanoparticles can be programmed for a particular particle diameter by varying the relative ratio of the amount of polymer to available surface area ($[PS\text{-}b\text{-}PAA]/n_m^s A_{Au}^{total}$). Because the properties of nanoparticles can be extremely sensitive to their local chemical and physical environment, we anticipate that the strategy outlined in this report will facilitate controlled application of nanoparticle materials where they might not ordinarily be stable or functional.

Acknowledgment. We thank the ACS Petroleum Research Fund (38303-G5) and National Institutes of Health (1 R21 EB003809-01) for financial support of this research.

Supporting Information Available: Details of characterization of polymers and nanoparticles, TEM images and histograms of before and after cross-linking the assembled shells, TEM images of unpurified samples, and additional TEM images which were used in obtaining histograms. This material is available free of charge via the Internet at http://pubs.acs.org.

References and Notes

(1) Savic, R.; Luo, L.; Eisenberg, A.; Maysinger, D. *Science* **2003**, *300*, 615−618.
(2) Kakizawa, Y.; Kataoka, K. *Adv. Drug Delivery Rev.* **2002**, *54*, 203−222.
(3) Malmsten, M. *Surfactants and Polymers in Drug Delivery*; Marcel Dekker: New York, 2002.
(4) Ottenbrite, R. M.; Kim, S. W. *Polymeric Drugs and Drug Delivery Systems*; Technomic Pub.: Lancaster, PA, 2001.
(5) Volkov, A. G. *Interfacial Catalysis*; Marcel Dekker: New York, 2003.
(6) Holmberg, K. *Surfactants and Polymers in Aqueous Solution*, 2nd ed.; John Wiley & Sons: Chichester, 2003.

(7) Goodwin, J. W. *Colloids and Interfaces with Surfactants and Polymers: An Introduction*; J. Wiley: Chichester, 2004.
(8) Toth, J. *Adsorption: Theory, Modeling, and Analysis*; Marcel Dekker: New York, 2002.
(9) Zhao, J. X.; Allen, C.; Eisenberg, A. *Macromolecules* **1997**, *30*, 7143−7150.
(10) Nagarajan, R.; Ganesh, K. *J. Colloid Interface Sci.* **1996**, *184*, 489−499.
(11) Wilhelm, M.; Zhao, C. L.; Wang, Y.; Xu, R.; Winnik, M. A.; Mura, J. L.; Riess, G.; Croucher, M. D. *Macromolecules* **1991**, *24*, 1033−1040.
(12) Currie, E. P. K.; Norde, W.; Stuart, M. A. C. *Adv. Colloid Interface Sci.* **2003**, *100*, 205−265.
(13) Halperin, A.; Tirrell, M.; Lodge, T. P. *Adv. Polym. Sci.* **1992**, *100*, 31−71.
(14) Marques, C.; Joanny, J. F.; Leibler, L. *Macromolecules* **1988**, *21*, 1051−1059.
(15) Singh, N.; Karim, A.; Bates, F. S.; Tirrell, M.; Furusawa, K. *Macromolecules* **1994**, *27*, 2586−2594.
(16) Qiu, X.; Wang, Z.-G. *J. Colloid Interface Sci.* **1994**, *167*, 294−300.
(17) Biver, C.; Hariharan, R.; Mays, J.; Russel, W. B. *Macromolecules* **1997**, *30*, 1787−1792.
(18) Watson, K. J.; Zhu, J.; Nguyen, S. T.; Mirkin, C. A. *J. Am. Chem. Soc.* **1999**, *121*, 462−463.
(19) Lai, J.-I.; Shafi, K. V. P. M.; Ulman, A.; Loos, K.; Lee, Y.; Vogt, T.; Lee, W.-L.; Ong, N. P. *J. Phys. Chem. B* **2005**, *109*, 15−18.
(20) Skaff, H.; Emrick, T. *Angew. Chem., Int. Ed.* **2004**, *43*, 5383−5386.
(21) Sakai, T.; Alexandridis, P. *Langmuir* **2004**, *20*, 8426−8430.
(22) Pyun, J.; Matyjaszewski, K.; Kowalewski, T.; Savin, D.; Patterson, G.; Kickelbick, G.; Huesing, N. *J. Am. Chem. Soc.* **2001**, *123*, 9445−9446.
(23) Lowe, A. B.; Sumerlin, B. S.; Donovan, M. S.; McCormick, C. L. *J. Am. Chem. Soc.* **2002**, *124*, 11562−11563.
(24) Kang, Y. J.; Taton, T. A. *J. Am. Chem. Soc.* **2003**, *125*, 5650−5651.
(25) Kang, Y. J.; Taton, T. A. *Angew. Chem., Int. Ed.* **2005**, *44*, 409−412.
(26) Ma, Q. G.; Wooley, K. L. *J. Polym. Sci., Part A: Polym. Chem.* **2000**, *38*, 4805−4820.
(27) Davis, K. A.; Matyjaszewski, K. *Macromolecules* **2001**, *34*, 2101−2107.
(28) Frens, G. *Nat. Phys. Sci.* **1973**, *241*, 20−22.
(29) Brown, K. R.; Walter, D. G.; Natan, M. J. *Chem. Mater.* **2000**, *12*, 306−313.
(30) Huang, H. Y.; Kowalewski, T.; Remsen, E. E.; Gertzmann, R.; Wooley, K. L. *J. Am. Chem. Soc.* **1997**, *119*, 11653−11659.
(31) Henselwood, F.; Liu, G. J. *Macromolecules* **1998**, *31*, 4213−4217.
(32) Zhang, L.; Eisenberg, A. *Science* **1995**, *268*, 1728−1731.
(33) See Supporting Information for further TEM images and histograms.
(34) Zhang, L. F.; Eisenberg, A. *J. Am. Chem. Soc.* **1996**, *118*, 3168−3181.
(35) Choucair, A.; Eisenberg, A. *Eur. Phys. J. E* **2003**, *10*, 37−44.
(36) Moffitt, M.; Vali, H.; Eisenberg, A. *Chem. Mater.* **1998**, *10*, 1021−1028.
(37) Jaramillo, T. F.; Baeck, S.-H.; Cuenya, B. R.; McFarland, E. W. *J. Am. Chem. Soc.* **2003**, *125*, 7148−7149.
(38) Lam, Y.-M.; Goldbeck-Wood, G.; Boothroyd, C. *Mol. Simul.* **2004**, *30*, 239−247.
(39) Tang, Y.; Liu, S. Y.; Armes, S. P.; Billingham, N. C. *Biomacromolecules* **2003**, *4*, 1636−1645.
(40) Wijmans, C. M.; Leermakers, F. A. M.; Fleer, G. J. *Langmuir* **1994**, *10*, 1331−1333.
(41) Bohner, M.; Ring, T. A.; Caldwell, K. D. *Macromolecules* **2002**, *35*, 6724−6731.
(42) Dan, N.; Tirrell, M. *Macromolecules* **1992**, *25*, 2890−2895.
(43) Hariharan, R.; Biver, C.; Mays, J.; Russel, W. B. *Macromolecules* **1998**, *31*, 7506−7513.
(44) Daoud, M.; Cotton, J. P. *J. Phys. (Paris)* **1982**, *43*, 531−538.
(45) Garvey, M. J.; Tadros, T. F.; Vincent, B. *J. Colloid Interface Sci.* **1974**, *49*, 57−68.
(46) Yu, K.; Eisenberg, A. *Macromolecules* **1996**, *29*, 6359−6361.
(47) Teraoka, I. *Polymer Solutions: An Introduction to Physical Properties*; John Wiley & Sons: New York, 2002.
(48) Dewalt, L. E.; Ou-Yang, H. D.; Dimonie, V. L. *J. Appl. Polym. Sci.* **1995**, *58*, 265−269.
(49) Dhoot, S.; Tirrell, M. *Macromolecules* **1995**, *28*, 3692−3701.
(50) Ligoure, C.; Leibler, L. *Macromolecules* **1990**, *23*, 5044−5046.

MA050400C